A New Molybdenum Nitride Catalyst with Rhombohedral MoS 2 Structure for Hydrogenation Applications

DATASET · SEPTEMBER 2015

READS
62

17 AUTHORS, INCLUDING:

Jj Zhang
Nankai University
981 PUBLICATIONS **50,490** CITATIONS
SEE PROFILE

Xiao-Dong Wen
Institute of Coal Chemsitry, Chinese Academy …
98 PUBLICATIONS **904** CITATIONS
SEE PROFILE

Yi Zhang
University of Nevada, Las Vegas
72 PUBLICATIONS **814** CITATIONS
SEE PROFILE

Yan Zhao
Université de Versailles Saint-Quentin
746 PUBLICATIONS **5,259** CITATIONS
SEE PROFILE

JACS
JOURNAL OF THE AMERICAN CHEMICAL SOCIETY
Article
pubs.acs.org/JACS

A New Molybdenum Nitride Catalyst with Rhombohedral MoS_2 Structure for Hydrogenation Applications

Shanmin Wang,*[,†,§,∥] Hui Ge,*[,‡] Shouli Sun,[¶] Jianzhong Zhang,[∥] Fangming Liu,[§] Xiaodong Wen,[‡,▽] Xiaohui Yu,[∥,⊥] Liping Wang,[†] Yi Zhang,[†] Hongwu Xu,[∥] Joerg C. Neuefeind,[○] Zhangfeng Qin,[‡] Changfeng Chen,[†] Changqin Jin,[⊥] Yongwang Li,[‡,▽] Duanwei He,[§] and Yusheng Zhao*[,†,∥,⊥]

[†]HiPSEC & Physics Department, University of Nevada, Las Vegas, Nevada 89154, United States
[‡]Institute of Coal Chemistry, Chinese Academy of Sciences, Taiyuan, Shanxi 030001, China
[§]Institute of Atomic & Molecular Physics, Sichuan University, Chengdu 610065, China
[∥]Los Alamos National Laboratory, Los Alamos, New Mexico 87545, United States
[⊥]Institute of Physics, Chinese Academy of Sciences, Beijing 100190, China
[¶]National Institute of Clean- & Low-Carbon Energy (NICE), Beijing 102209, China
[▽]Synfuels China, Beijing, 100195, China
[○]Oak Ridge National Laboratory, Oak Ridge, Tennessee 37831, United States

Supporting Information

ABSTRACT: Nitrogen-rich transition-metal nitrides hold great promise to be the next-generation catalysts for clean and renewable energy applications. However, incorporation of nitrogen into the crystalline lattices of transition metals is thermodynamically unfavorable at atmospheric pressure; most of the known transition metal nitrides are nitrogen-deficient with molar ratios of N:metal less than a unity. In this work, we have formulated a high-pressure route for the synthesis of a nitrogen-rich molybdenum nitride through a solid-state ion-exchange reaction. The newly discovered nitride, 3R−MoN_2, adopts a rhombohedral *R*3*m* structure, isotypic with MoS_2. This new nitride exhibits catalytic activities that are three times more active than the traditional catalyst MoS_2 for the hydrodesulfurization of dibenzothiophene and more than twice as high in the selectivity to hydrogenation. The nitride is also catalytically active in sour methanation of syngas with >80% CO and H_2 conversion at 723 K. Our formulated route for the synthesis of 3R−MoN_2 is at a moderate pressure of 3.5 GPa and, thus, is feasible for industrial-scale catalyst production.

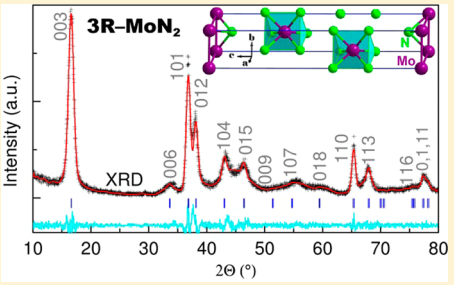

INTRODUCTION

Heterogeneous catalysis plays a central role in key chemical processes associated with petrochemical and renewable energy generation. Since the first success in catalytic liquefaction of coal in 1920s,[1] MoS_2−based catalysts have been extensively studied and used for hydrotreating of fossil fuels,[1] sour methanation of syngas,[2] electrocatalysis for water splitting,[3] and solar energy conversion.[4] The excellent catalytic performances of this family of catalysts are primarily attributed to the layered structure of MoS_2 in which the interlayers of Mo and S are held together by weak van der Waals forces.[5,6] This structural characteristic allows producing a variety of nanoclusters with highly exposed active edge sites on the S−Mo−S sandwich layer. The catalytic activity of the exfoliated MoS_2 thin layers,[7] for example, is three times that of the dispersed MoS_2 on a silica mesoporous substrate.[8] In addition, the edge sites of the S−Mo−S layer can absorb promoter species, such as Co and Ni, significantly improving the catalytic performances.[1,8]

Despite several decades of searches for other catalysts, the transition metal (TM) disulfides remain the most studied and used catalysts in deep hydroprocessing of fossil fuels including hydrodesulfurization (HDS) and hydrodenitrogenation (HDN).[1,9] Over the past decade, however, TM nitrides have attracted considerable attention because they exhibit a number of unique and advanced catalytic properties for hydrotreating (e.g., Mo_2N and W_2N)[10] and photo- and electrochemical-catalysis (e.g., δ−MoN, Mo_2N, and Ta_3N_5),[11−13] although none of them adopts a layered structure. One important property is their excellent resistance to corrosion by sulfur, a common catalyst poison;[1,2] hence, they can be used for sour catalysis applications. In some reactions such as dehydrogenation and hydrogenolysis, molybdenum nitride shows similar catalytic activities as platinum-group catalysts.[10,12,14,15] Thus, nitrogen-rich TM nitrides, particularly those of MoS_2-type, may hold

Received: February 11, 2015
Published: March 23, 2015

DOI: 10.1021/jacs.5b01446
J. Am. Chem. Soc. 2015, 137, 4815−4822

great promise as the next-generation catalysts for a wide range of applications.

Preparation of nitride-rich TM nitrides is challenging because incorporation of nitrogen into the crystal lattice of TMs is often thermodynamically unfavorable at atmospheric pressure.[16] As a result, most of the known TM nitrides are nitrogen-deficient with $x \leq 1$ in TMN_x, in spite of the fact that TMs often exhibit oxidation states exceeding +3. To date, reports on TM nitrides with $x > 1$ are rather fragmentary, sometimes even contradictory, especially on their crystal structures. In the binary Mo−N system, three different phases with varying nitrogen concentrations have been reported: tetragonal β−MoN_x with $x \leq 0.5$ (e.g., Mo_2N[17]), cubic γ−MoN_x with $0.5 \leq x < 1$ (e.g., Mo_3N_2[18]), and hexagonal δ−MoN_x with $x \geq 1$ (e.g., MoN[19]). Also noted is that Mo_5N_6 is the only nitride with $x > 1$ in the binary system Mo−N.[19]

Using high-pressure techniques, a number of novel nitrogen-rich TM nitrides have recently been synthesized[20] including new polymorphs of Zr_3N_4,[21] Hf_3N_4,[21,22] Ta_2N_3,[23] and Ta_3N_5,[24] and noble metal dinitrides (OsN_2, IrN_2, and PtN_2).[25,26] Successful high-P synthesis of nitrides with higher oxidation states demonstrates that pressure can effectively promote the role of d-electrons in chemical bonding with nitrogen. However, the required pressures in most of the previous synthetic routes are relatively high, in a range of 11−50 GPa, which is beyond the current technological capability for massive, industrial-scale production. Hexagonal ReN_2 has recently been synthesized through a solid-state reaction at 7.7 GPa and is the only nitride possessing a layered MoS_2−type structure.[27] To date, no nitrogen-rich nitride has been synthesized in the Mo−N system, although an oxidation state as high as +6 occurs in other chemical systems (e.g., MoO_3).

Most recently, we successfully synthesized stoichiometric CrN and a series of novel nitrogen-rich tungsten nitrides (e.g., W_2N_3 and W_3N_4) through a newly formulated solid-state ion-exchange reactions between Na_2XO_4 (X = Cr, W) and hBN at pressures up to 5 GPa.[28,29] In this work, we have extended this high-P methodology to the Mo−N system with a focus on nitrogen-rich phases, leading to the discovery of a novel nitride, MoN_2. Here, we report the high-P synthesis, structural characterization, and catalytic property measurements of this novel nitride compound.

EXPERIMENTAL SECTION

Starting Materials, Synthesis, and Purification. High-purity Na_2MoO_4 (>99.5%, ∼50 μm) and hBN (>99.9%, ∼50 μm) powders in the molar ratio Na_2MoO_4:BN = 1:2 were homogeneously mixed for the synthesis of molybdenum nitrides. Na_2MoO_4 was obtained by dehydration of commercially available $Na_2MoO_4{\cdot}2H_2O$ in a muffle furnace at 473 K for 12 h.

High P-T synthetic experiments were carried out using a DS 6 × 14 MN cubic press at Sichuan University, China.[30] In each experiment, the powder mixture was compacted into a cylindrical pellet of 12 mm in diameter and 10 mm in height, which was then sealed within a molybdenum capsule to prevent possible contamination. The detailed experimental procedures have been described elsewhere.[30] The run products were washed with distilled water to remove the byproduct $NaBO_2$ and unreacted Na_2MoO_4, followed by drying in an oven at 348 K. To obtain a nitrogen-rich nitride, the synthesis was performed at a relatively low temperature of 773 K to avoid potential high-T degassing. For each experimental run, the reaction was incomplete even after a prolonged heating of 8−10 h, and the insoluble hBN impurity was identified in the purified sample (see Supporting Information Figure S1). Therefore, a two-step reaction route was adopted to eliminate hBN; the purified run products from the first-step reaction, the nitride and unreacted hBN, were mixed with additional Na_2MoO_4 in a weight ratio of ∼1:2 for the second-step synthesis.

Characterization. The final products were characterized by X-ray diffraction (XRD) with Cu Kα radiation and time-of-flight neutron powder diffraction (NPD) performed at the beamline of Nanoscale−Ordered Materials Diffractometer (NOMAD) of SNS, Oak Ridge National Laboratory.[31] The crystal structure was determined from Rietveld analysis of the X-ray and neutron diffraction data using the GSAS software.[32]

Thermogravimetric mass spectrometer (TG−MS) measurements were carried out in an Ar atmosphere on a Setaram TGA-92 instrument equipped with an OmniStar-200 quadrupole mass spectrometer, which was used to qualitatively monitor the outlet gases at high temperatures. In air, a simultaneous TG-DTG (derivative thermogravimetry) measurement was performed to study the oxidation of the new nitride. For each experimental run, phase-pure nitride powders (∼10 mg) were loaded, and automatically heated to a target temperature of 1073 K at a rate of 10 K·min^{-1} and soaked for 30 min before quenching the sample to room temperature. For the TG−MS measurement, the mass-to-charge ratios, m/z, were qualitatively recorded to monitor N_2 and nitrogen oxide gases, such as N_2O, NO, and NO_2, for possible oxidation. The nitrogen content, x, in the obtained MoN_x was determined by the TGA−DTG via oxidation of MoN_x.

Microstructures of the purified sample were characterized by a field emission scanning electron microscopy (SEM) and high-resolution transmission electron microscopy (HRTEM). Energy-dispersive X-ray (EDX) was employed for compositional analyses and the selected area electron diffraction (SAED) was carried out to confirm the crystal structure. X-ray photoelectron spectroscopy (XPS) measurements were performed to determine the electronic structure of the new phase. Using the Archimedes method, the density of the sample was measured on a bulk sample sintered at 3.5 GPa and 753 K for 8 h.

The specific surface area and pore structures of the nitride catalyst were determined from physisorption of N_2 by using the BET and BJH methods at 77 K and low relative pressure (P/P_0) of 0−0.3.[33,34] The measurement was performed in a Tristar−3000 instrument. Traditional MoS_2 catalyst was also measured for comparison. Before measurement, the two catalysts were treated at 473 K in a vacuum for 6−8 h to remove possible impurity gases adsorbed from the air.

The temperature-programmed desorption (TPD) measurement of the pre-adsorbed CO gas was used to determine the concentration of active Mo atoms in the catalysts. Experiment was conducted in a TP-5080 quartz microreactor. To remove the possible adsorbed impurity gases, the samples (∼100 mg) were treated at 623 K for 30 min in a He atmosphere with a flow rate of 30 mL·min^{-1}, followed by cooling the sample to 323 K over a period of 60 min. Before desorption, chemisorption of CO was carried out at 323 K in a He atmosphere with a 0.4% volume fraction of CO. The mixed gases were flowed for 60 min at a flow rate of 50 mL·min^{-1} to have a sufficient adsorption. In order to eliminate the physisorbed CO, the catalyst was then flushed in a He flow at 323 K for 60 min with a flow rate of 30 mL·min^{-1}. The subsequent desorption process of CO was monitored at temperatures up to 673 K with a heating rate of 10 K·min^{-1}. In all these processes, the volume of the desorbed CO was determined by a quadrupole mass spectrometer, OmniStar GSD-320, which was pre-calibrated by using standard mixed gases of He and CO (see ref 35 for details) and the calibrated parameter is ∼13.147 mol of CO per unit area.

The catalytic hydrodesulfurization (HDS) of dibenzothiophene (DBT) using MoN_2 and MoS_2 catalysts was carried out in a high-P batch reactor/autoclave at 623 K and 6 MPa in H_2 atmosphere. Before the experiment, DBT was dissolved into decalin as the feedstock in a weight fraction of 500 ppm and the total feed oil is 90.0 g with a volume of 101.1 mL. For each experimental run, 0.3 g of catalyst was placed in the reactor with a stirring speed of 300 rpm. At 623 K, the reaction was followed for 48 h by sampling the products every 8 h. Sour methanation of the syngas was performed in a continuous-flow and fixed-bed reactor. The nitride sample used in the experiment was 0.25 g, which was sandwiched between quartz fibers in the middle of the reactor. A syngas mixture of H_2, CO, H_2S, and N_2 was used as the

DOI: 10.1021/jacs.5b01446
J. Am. Chem. Soc. 2015, 137, 4815−4822

starting reactants in a molar ratio of H_2:CO:H_2S:N_2 = 47.3:47.3:1.2:5.2. The experiment was conducted at 3 MPa and 723 K with an hourly space velocity of 5000 h^{-1}. For both HDS and methanation experiments, the outlet gases were quantitatively analyzed by an online gas chromatograph (see refs 36 and 37 for details).

RESULTS AND DISCUSSION

Figure 1a shows an XRD pattern of the purified product synthesized at 3.5 GPa and 753 K for 20 h. As discussed below,

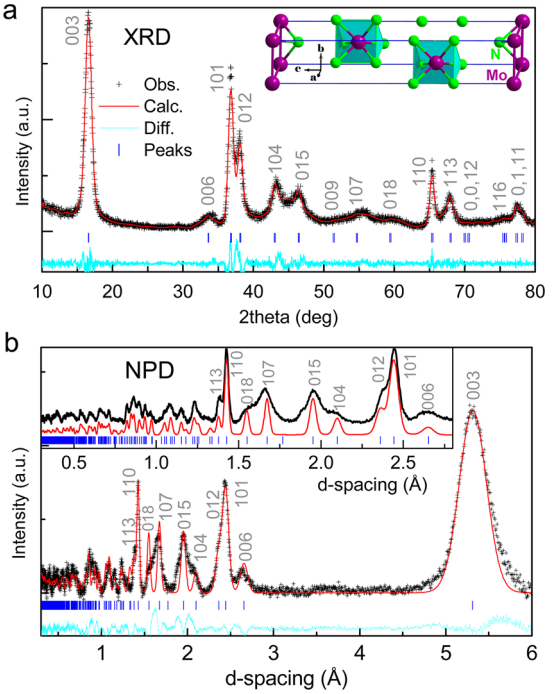

Figure 1. Refined XRD and NPD patterns of 3R−MoN_2. (a) XRD data collected using a Cu Kα radiation. Inset is a polyhedral view of the 3R−MoN_2 structure. (b) NPD data collected at a Bragg scattering angle of 30°. A higher-resolution NPD pattern is plotted in the inset, which was collected at a 66° scattering angle. The observed and calculated patterns are shown in black and red, respectively. The positions of allowed Bragg reflections are denoted by blue tick marks. The sample synthesis was performed at 3.5 GPa and 753 K for 20 h through a two-step reaction (see Experimental Section). The misfit in the d-spacing range of 1.5−2.1 Å is mainly attributed to significant peak broadening in a subset of reflections, notably 104, 015, 107 and 018, which originates from the layer stacking disorder (refs 5 and 49).

MoN_2 was formed through the following high-P solid-state reaction

$$Na_2MoO_4 + 2BN = MoN_2 + 2NaBO_2 \quad (1)$$

which may simply be viewed as an ion-exchange process between Mo^{6+} and B^{3+}. We have also prepared W_2N_3 and CrN at high P and T conditions through similar reactions.[28,29,38] In all the experimental runs performed, reaction 1 was incomplete even after a prolonged heating of 8−10 h (see Supporting Information Figure S1), indicating that the reaction is kinetically sluggish. The nitride sample can be purified by washing the unreacted Na_2MoO_4 and reaction by-product, $NaBO_2$, with water, leaving behind hBN as the only impurity phase in the run product. The unwanted hBN can further be eliminated in a two-step reaction route, described in detail in the Experimental Section, leading to a phase-pure nitride after a second washing. The obtained run product displays a number of Bragg reflections that do not belong to any of the known molybdenum nitrides such as Mo_2N, Mo_3N_2, MoN, Mo_5N_6, and their solid solutions (Figure 1a).[17,19,39] Instead, the diffraction peaks can be indexed by a rhombohedral structure with the lattice parameters a = 2.854 (1) Å and c = 15.938 (2) Å. Further, the XRD pattern of this new nitride resembles those of WN_2,[40] 3R−MoS_2,[5] and LiXN_2 (X = W and Mo)[41,42] with a symmetry of either $R\bar{3}m$ (No. 166) or $R3m$ (No. 160). In most molybdenum and tungsten nitrides, trigonal-prismatic coordination [XN_6] (X = Mo and W) is preferably adopted for X atoms.[38,41,42] On the other hand, the $R\bar{3}m$ structure only contains the octahedral coordination [XN_6]. Therefore, the space group $R3m$ (No. 160), in which X atoms reside in the trigonal prismatic sites, was used for Rietveld analysis of the XRD data.

In the $R3m$ structure, three crystallographically distinct positions are allowed for Mo with multiplicities of 3, 9, and 18.[43] For most reported binary TM−N compounds, as a constraint, their densities typically cannot exceed those of their parent metals. Thus, the Wyckoff site 3a (0, 0, z), which has the lowest number of multiplicity, is the only possible position for Mo in this structure. Because the XRD intensities of molybdenum nitride primarily originate from X-ray scattering of Mo, N was omitted from the structure model during the initial Rietveld analysis. The thus-refined position for Mo is 3a (0, 0, z) with z = 0. Since further treatment of the as-purified nitride at 3.5 GPa and 1523 K led to its decomposition into a known hexagonal δ−MoN (see Supporting Information Figure S6), the new nitride phase must be nitrogen−rich with y: $x > 1$ in Mo_xN_y. However, as an upper limit, the x:y ratio should not be greater than 2 because the highest possible oxidation state for Mo is +6. In addition, two independent 3a (0, 0, z) sites are allowed for N to achieve the experimental density of $\rho_0 \approx 4.97$ g·cm^{-3}, determined using a well-sintered bulk sample (see Supporting Information Figure S8 and Table S2). On the basis of these considerations, the stoichiometry of this new nitride compound is determined to be Mo_3N_6 (i.e., MoN_2). This formula is in good agreement with the nitrogen concentration obtained from thermogravimetric measurement, $x \approx 2.2$ (3) in MoN_x, which will be discussed latter.

To further resolve the crystal structure, we conducted powder neutron diffraction experiment on the purified run product. Unlike X-rays, the N atom is an excellent neutron scatterer with a coherent scattering length of ~9.36 fm, which is ~40% larger than that of Mo (~6.72 fm).[44] Therefore, the atomic positions of nitrogen can be well determined from Rietveld analysis of neutron diffraction data (Figure 1b). The thus-obtained coordinates for nitrogen are 3a (0, 0, z) with z = 0.258(1) and z = 0.402(2), indicating that Mo ions are in trigonal-prismatic coordination, [MoN_6] (see inset of Figure 1). The refined structural parameters of MoN_2 are summarized in Table 1. As shown in Figure 1, the calculated X-ray and neutron patterns using this structure model agrees well with the observed patterns. Because the resolved structure for MoN_2 is isotypic with that of rhombohedral 3R−MoS_2,[5] we denote it as 3R−MoN_2. Evidently, a subset of diffraction peaks in Figure 1, such as 104, 015, 107, and 018, exhibit significant broadening, whereas other peaks (such as 003, 101, and 110) remain sharp (see Supporting Information Figure S3). In addition, some reflections in the low d−spacing (i.e., large 2θ) region either are too weak to be seen (e.g., 009 and 116) or show significant reduction in the diffraction intensity (e.g., 107 and 018). These phenomena, frequently occurred in layer-structured systems in

DOI: 10.1021/jacs.5b01446
J. Am. Chem. Soc. 2015, 137, 4815−4822

Table 1. Summary of Structural Parameters for MoN_2 Phases Determined by Rietveld Analyses of X-ray and Neutron Diffraction Data Taken at Ambient Conditions

	3R−MoN_2
formula	Mo_3N_6
space group	rhombohedral , *R*3*m* (No. 160)
cell parameters [Å]	$a = b = 2.854$ (1), $c = 15.938$ (2)
cell volume [Å^3]	112.426
density [g·cm^{-3}]	5.492
Mo Wyckoff site	Mo1:3*a*, (0, 0, 0.000 (1))
N Wyckoff sites	N1:3*a*, (0, 0, 0.258 (1)), N2:3*a*, (0, 0, 0.402 (2))
d_{Mo-N} [Å]	1.976, 2.037
$D_{interlayer}$ [Å][a]	5.313 (1)
$D_{layer\ distance}$ [Å][a]	3.017 (1)
R_P, wR_P [%] (NPD)	3.2, 5.3

[a] $D_{interlayer}$ is the distance between the two nearest neighboring Mo planes, and $D_{layer\ distance}$ corresponds to the distance between the N planes.

nanocrystalline forms such as nanocrystalline MoS_2,[45−48] can mainly be attributed to the layer stacking disorder and atomic disorder on the surface of nanocrystals.[5,45,49] As will be discussed below, as-prepared 3R−MoN_2 is also in a nanocrystalline form with layer stacking disorder. It is worthwhile to mention that 3R−MoN_2 and MoS_2 have almost the same core-level Mo 3d and Mo 3p binding energy (see X-ray photoelectron spectroscopy measurement in Supporting Information Figures S4 and S5). The determined valence state for Mo is +3.5 in both 3R−MoN_2 and MoS_2, inferring a peculiar $4d^{2.5}$ electronic structure. Note that a non-integral valence state (< +4) has previously been reported in MoS_2.[50] Further computational work is warranted to quantify and understand the interesting electronic structures in 3R−MoN_2.

The microstructures obtained from high-resolution transmission electron microscopy (HRTEM) are shown in Figure 2. As expected for a layered compound, the grains of 3R−MoN_2 exhibit a laminated morphology with a crystallite size of ∼100−200 nm and an edge thickness of ∼10−25 nm (see Figure 2a). Figure 2b shows the atomic-scale crystalline edge. Along the *c* axis, the Mo atoms show a fringe pattern with a distance of ∼0.53 nm, which corresponds to the (003) plane (also see Table 1). The crystalline edge is also nano-twinned and nano-twisted, corresponding to layer stacking disorder of the N−Mo−N interlayers. As shown in Figure 2c, (101) lattice fringes with a *d*-spacing of ∼0.25 nm are clearly revealed; this *d*-spacing is close to the refined value of 2.4716 Å (i.e., $a\sqrt{3}/2$, see Table 1). Consistent with the resolved structure for 3R−MoN_2, the HRTEM image (inset in Figure 2c) shows a clear hexagon formed by Mo atoms. Also noted is that the crystals along (101) plane show a ribbonlike morphology with distinct grain boundaries. Figure 2d shows a selected-area electron diffraction pattern; four diffraction rings are identified, and they correspond to the planes (003), (101), (012), and (104).

Thermal stabilities of the new nitride were studied by simultaneous thermogravimetry−derivative thermogravimetry (TG−DTG), as shown in Figure 3. In air, there is an obvious weight increase at ∼610 K, indicating the onset of oxidation, which is comparable to that of MoS_2 (∼623 K). Evidently, the oxidation process is complete at ∼780 K when a plateau value is reached, and the final product is MoO_3 (see Supporting Information Figure S7). The nitrogen concentration in the nitride can be readily determined from thermogravimetric

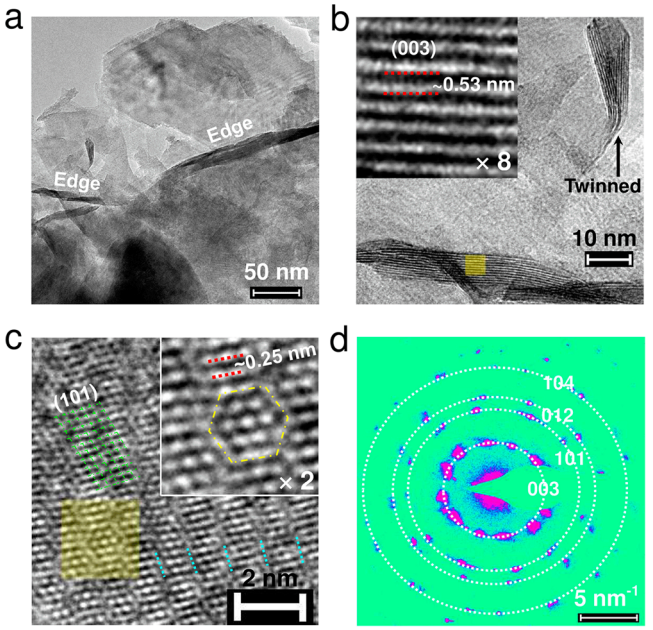

Figure 2. HRTEM images and electron diffraction pattern for 3R−MoN_2. (a) Plate-shaped crystals with laminate edges. (b) Atomic-scale images of the N−Mo−N interlayers, that is, the (003) plane, and (c) the (101) plane. The inset in both (b) and (c) are the enlarged portions of the regions highlighted in yellow. Dotted double red lines indicate the d-spacing for the fingerprints of (003) and (101) planes. Dotted cyan lines in (c) denote the grain boundaries. (d) Selected area electron diffraction, SAED. The observed four diffraction rings correspond to the lattice planes of (003), (101), (012), and (104).

data,[38] and the obtained value is $x = 2.2(3)$ in MoN_x. The sublimation of MoO_3 happens at ∼1000 K as the weight decreases steeply. As shown in Figure 3b, in an Ar atmosphere, the nitrogen degassing of 3R−MoN_2 starts at ∼850 K, which gives rise to a more stable product of hexagonal δ−MoN (see Supporting Information Figure S6)[51] via the reaction

$$MoN_2 = MoN + \frac{1}{2}N_2 \quad (2)$$

The desorption of NO and N_2O occurs in the temperature region of ∼400−450 K, which results from the reaction between MoN_2 and O_2 adsorbed on the surface. This indicates that the NO chemisorption analysis, a common method used for the determination of coordinately unsaturated Mo sites of MoS_2-based catalysts,[52] cannot be used for 3R−MoN_2, which is discussed below in more detail.

The catalytic properties of 3R−MoN_2 were measured in hydrodesulfurization (HDS) of dibenzothiophene (DBT), a common sulfur-bearing compound in diesel fuels that is more difficult to be hydrodesulfurized compared with thiols and thiophenes.[1] For comparison, traditional catalyst MoS_2 and 3R−MoN_2 containing BN impurity were also tested. For Mo-based catalysts, the surface area with the coordinately unsaturated Mo sites is catalytically active centers. Equally important is the pore structure of the catalyst, which also affects the surface area. For a given catalyst, the distribution of pore sizes may be such that the internal surface area is completely inaccessible for large reactant molecules and, which may restrict the rate of conversion to products by impeding the diffusion of reactants and products throughout the porous medium.[53,54] We examined the surface area and pore size for 3R−MoN_2 and MoS_2 using the BET and BJH analyses of N_2 physisorption

DOI: 10.1021/jacs.5b01446
J. Am. Chem. Soc. 2015, 137, 4815−4822

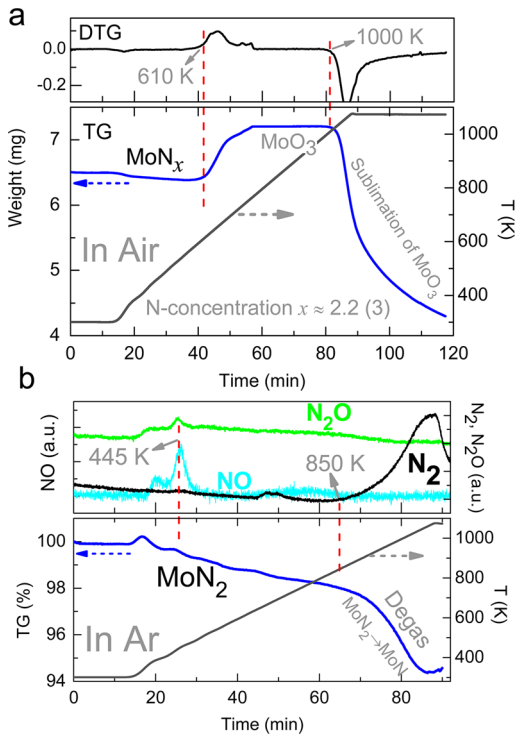

Figure 3. Thermal stability analysis. (a) Thermogravimetry/differential thermal analysis, TG/DTG, performed in air. Oxidation of MoN_2 starts at ~610 K, and the final product is MoO_3, which starts sublimating at a temperature of ~1000 K. The derived nitrogen concentration is $x = 2.2(3)$ in MoN_x. (b) TG measurement of high-temperature degassing of N_2 in an Ar atmosphere. The outlet gases are qualitatively traced during heating. At 400–445 K, the surface absorbed O_2 is released in forms of NO and N_2O. The significant degassing of N_2 happens at ~850 K.

performed at 77 K and low relative N_2 pressure (P/P_0) of 0–0.3 (see Supporting Information Figure S11).[34] The obtained data are listed in Table 2. For both catalysts, the measured specific surface area is ~3–10 $m^2 \cdot g_{cat}^{-1}$, ~10–50 times smaller than those reported for the promoted and supported MoS_2–based catalysts.[7,36,55,56] Similar differences in the pore sizes are also found.[55] Such small values are unfavorable for achieving a high catalytic activity as already reported in well-designed catalysts.[7,36,55,56] Compared with MoS_2 used in our comparative study, 3R–MoN_2 possesses a larger specific surface area, although the pore size is nearly identical (see Table 2). Based on the measured specific surface area, the catalytic activity for MoN_2 can be normalized and, to a first approximation, assessed relative to the traditional MoS_2. For a more accurate assessment, we determined the active Mo sites per mole of each of the two catalysts based on CO uptake measurement, i.e., chemisorption-desorption of CO molecules on the catalyst's surface,[34,52,57] and experiments were performed at similar conditions (see Experimental Section for detail). Because of the structural similarity, the two catalysts show similar desorption spectra characterized by a main peak and a weaker satellite peak (Figure 4a), corresponding to two different adsorption sites. These characteristics have theoretically been attributed to coordinately unsaturated $(\bar{1}010)$ and $(10\bar{1}0)$ Mo sites on the edge of hexagonally packed slabs.[57] For 3R–MoN_2, the main peak occurs at a higher temperature (~440 K) than that of MoS_2 (~420 K), indicating that CO molecules are more tightly bounded at unsaturated $(\bar{1}010)$ Mo sites. By analysis of the CO uptake data, the molar volume for the absorbed CO can be quantified, and they are listed in Table 2 (also see Supporting Information Figure S12). The calculated ratio between 3R–MoN_2 and MoS_2 is CO_{3R}: CO_{MoS_2} = 1.35:1, which is used to normalize the catalytic activity between two catalysts. It is worthwhile to point out that an NO uptake test was initially attempted, but the gas reacted with MoN_2 to form N_2O (also see Figure 3b).

Figure 4b shows the results of HDS of DBT at 623 K using 3R–MoN_2 and MoS_2. Strikingly, at the early stages of HDS, the DBT conversion using phase-pure 3R–MoN_2 is more than four times higher than the conversion using MoS_2. Overall, after 2 days of the reaction, ~97% DBT conversion was achieved using 3R–MoN_2, whereas only 50% conversion was attained using MoS_2. The catalytic activity can more generally be described by a pseudo-first order rate constant, k, for the HDS of DBT (Figure 4c), given by

$$\ln \frac{C_t}{C_0} = -\frac{k \cdot (n_{CO})}{V_{oil}} \cdot t \qquad (3)$$

where C_t/C_0 denotes the ratio of DBT concentration between reaction time t and $t = 0$, V_{oil} is the volume of the feed solution (i.e., 101.1 mL of DBT and decalin oil), and n_{CO} is the number of active Mo sites, which can be calculated from analysis of the CO uptake data (see Table 2) and also serves as a normalization parameter the k value. The obtained value for MoN_2 is $k = 0.141$ $L_{oil} \cdot (mol_{CO})^{-1} \cdot s^{-1}$, which is more than three times higher than that of MoS_2 (~0.044 $L_{oil} \cdot (mol_{CO})^{-1} \cdot s^{-1}$). Therefore, 3R–$MoN_2$ is substantially more catalytically active than the traditional MoS_2 catalyst, presumably due to unsaturated Mo atoms that are more energetically enhanced at $(\bar{1}010)$ sites in 3R–MoN_2 (see Figure 4a). It is worth mentioning that, to determine the intrinsic catalytic activity, neither promoter nor support was used for 3R–MoN_2 and MoS_2. However, the catalytic activity of 3R–MoN_2 is significantly deteriorated in the presence of *h*BN impurity

Table 2. Summary of CO Uptake Data, BET Surface Area, and Pore Volume and Width for 3R–MoN_2 and MoS_2 Catalysts[a]

catalyst	3R–MoN_2	MoS_2	ratio 3R:MoS_2
BET surface area [$m^2 \cdot g_{cat}^{-1}$]	8.656 (9)	3.699 (5)	2.34
pore volume [$\mu \cdot m^3 \cdot g_{cat}^{-1}$]	0.036	0.016	2.25
Average pore width [nm]	16.54	17.14	0.96
CO uptake [$\mu \cdot mol_{CO} \cdot g_{cat}^{-1}$]	47.19	34.97	1.35
CO/Mo [$\times 10^{-3}$ $mol_{CO} \cdot mol_{Mo}^{-1}$][b]	5.850	5.598	1.05
k [$L_{oil} \cdot mol_{CO}^{-1} \cdot s^{-1}$]	0.141	0.044	3.20

[a]Also listed are the pseudo-first-order rate constant, k, which are normalized to the active Mo sites. [b]CO in the CO/Mo ratio denotes the molar volume of CO adsorbed onto the Mo sites (i.e., coordinately unsaturated Mo sites). The ratio CO/Mo represents the percentage of catalytically active Mo sites.

DOI: 10.1021/jacs.5b01446
J. Am. Chem. Soc. 2015, 137, 4815–4822

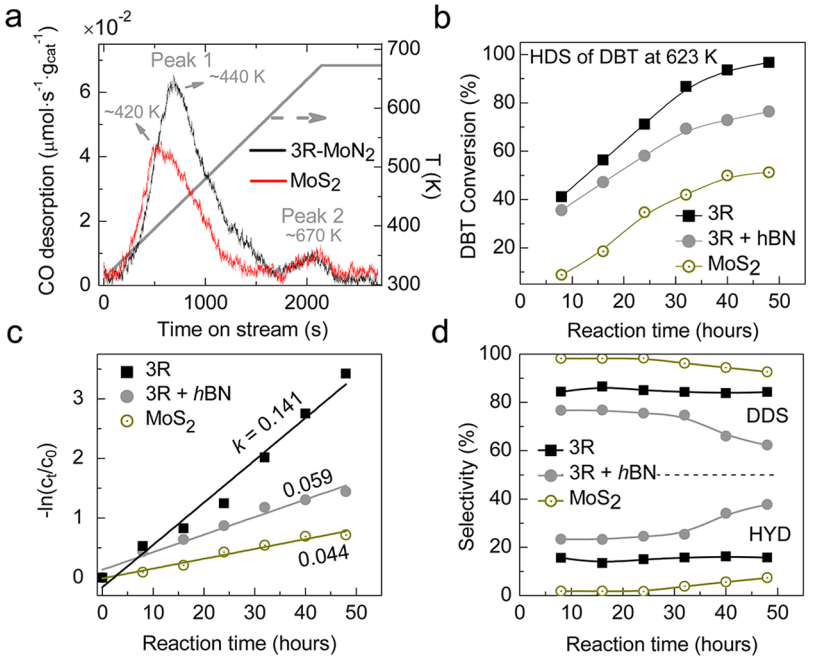

Figure 4. Catalytic activities of 3R−MoN_2 in the hydrodesulfurization (HDS) of dibenzothiophene (DBT). Traditional catalyst MoS_2 was also tested for comparison. (a) Temperature-programmed desorption (TPD) of CO to determine the amounts of active Mo sites. Before experiment, the catalysts were pre-exposed to CO gas at 323 K for 60 min to absorb CO molecules and form Mo−CO bonds with active Mo sites, including coordinately unsaturated $(\bar{1}010)$ and $(10\bar{1}0)$ Mo sites. (b) HDS of DBT at 623 K and 6 MPa in H_2 atmosphere. (c) Relative DBT concentration, c_t/c_0, as a function of reaction time t. The normalized pseudo-first-order rate constant, k, was deduced by linear fits. (d) The measured selectivity of direct desulfurization (DDS) and hydrogenation (HYD) in the HDS of DBT (see Supporting Information Figures S9−S14).

(see XRD in Supporting Information Figure S9), indicating that nonmetallic impurities would lead to the reduction of active sites for the catalytic reaction. On the other hand, as shown in Figure 4d, the BN−MoN_2 catalyst exhibits an enhanced catalytic activity for the hydrogenation (HYD) of DBT to form sulfur-free products of cyclohexylbenzene (CHB) and bicyclohexyl (BCH) (see Supporting Information Figure S10). For direct desulfurization (DDS), biphenyl (BP) is the only product. Compared with MoS_2, the BN−MoN_2 catalyst is 6−12 times more selectivity to HYD. Besides, the phase-pure 3R−MoN_2 exhibits selectivity to HYD that is 2−7 times higher than MoS_2, close to the case of the promoted and supported Ni−MoS_2/Al_2O_3, a widely used commercial catalyst.[58] For both BN−MoN_2 and phase-pure MoN_2, the reported ranges of selectivity reflect their sensitivity to reaction time (Figure 4d), which may be associated with the DBT concentrations, as the latter decrease with increasing reaction time. Clearly, 3R−MoN_2 is an intrinsic supercatalyst for the hydrogenation, which is highly attractive from the perspectives of ultra-deep hydrodesulfurization of fossil fuels.

The catalytic activities were also evaluated using MoN_2 as a catalyst in the sour methanation of syngas, a synthesis gas consisting primarily of CO, H_2, and sour gases such as H_2S, which often causes catalyst poisoning when traditional Ni-based catalysts were used.[2] Our preliminary results of sour methanation of syngas are shown in Figure 5a. At the early stages of the reaction, more than 80% conversion was achieved for both H_2 and CO at 723 K in a H_2S atmosphere. As the reaction products, the outlet gases of CH_4 and CO_2 were detected in a molar ratio CH_4: $CO_2 \approx 1{:}1$, indicating a sour methanation process given by

$$2H_2 + 2CO = CH_4 + CO_2 \quad (4)$$

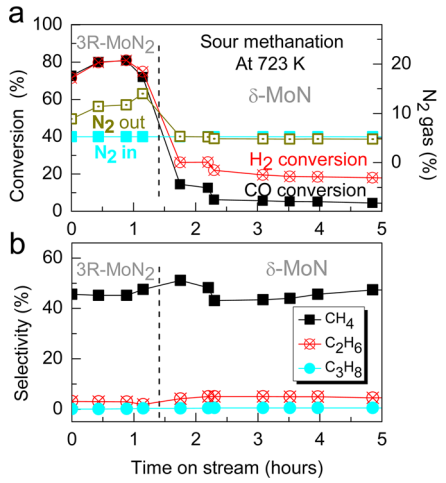

Figure 5. Catalytic performance of 3R−MoN_2 in sour methanation. (a) Conversion of H_2 and CO as a function of reaction time at 723 K. Volume fractions of the input and output N_2 gas are plotted to show the high-T degassing of MoN_2 and the subsequent formation of δ−MoN. (b) The measured selectivity of CH_4, C_2H_6, and C_3H_8 in the sour methanation. No promoters or supporting substrates were used in the catalytic measurements.

The observed high catalytic activity of 3R−MoN_2 for sour methanation is comparable to that obtained recently using a Zr-promoted MoS_2 catalyst[2] and is significantly higher than the catalytic activities of Co−MoS_2/γ−Al_2O_3.[37] However, the reaction 4 lasted for only 1.4 h, after which the conversion for both H_2 and CO was lowered drastically. Concurrently, as shown in Figure 5a, the excessive N_2 was released as the reaction proceeds. Most likely, this is due to the degassing of 3R−MoN_2 at 723 K, which converts 3R−MoN_2 to hexagonal

DOI: 10.1021/jacs.5b01446
J. Am. Chem. Soc. 2015, 137, 4815−4822

δ−MoN. As the N_2 output is stabilized at the input level, H_2 and CO are converted into CH_4 in a molar ratio of H_2:CO ≈ 3:1, which is typical of a traditional methanation reaction

$$3H_2 + CO = CH_4 + H_2O \quad (5)$$

Obviously, 3R−MoN_2 is catalytically more active and efficient than δ−MoN in the methanation of syngas. The 3R−MoN_2 and δ−MoN catalysts, however, show similar selectivity for CH_4 as seen in Figure 5b. In practice, the syngas can be produced by gasifying coal and biomass. The sour methanation is an essential process for upgrading such low-grade energy sources. The search for new catalysts with high poisoning resistance is highly demanded from the perspectives of enhanced process and energy efficiency. As a candidate catalyst, the 3R−MoN_2 holds great promise for future sour methanation applications.

To the best of our knowledge, 3R−MoN_2 is the first binary nitride having a rhombohedral MoS_2 structure and is only the fifth binary nitride in bulk forms exhibiting the stoichiometry of XN_2, after noble metal nitrides ReN_2, OsN_2, IrN_2, and PtN_2.[25,27,59] As expected, the layer-structured 3R−MoN_2 is intrinsically an excellent catalyst. It is sulfur-poisoning tolerant and exhibits superior catalytic activities over the traditional MoS_2-based catalysts for the HDS of DBT, even without the presence of a promoter or a supporting substrate. It is conceivable that the discovery of 3R−MoN_2 may open new opportunities for developments of highly active, MoN_2-based catalysts through the introduction of promoter species (e.g., Co, Ni, and Zr) and supporting substrates (e.g., Al_2O_3 and SiO_2), as already demonstrated for the MoS_2 catalysts.[1,2] As another nitride of the group 6 metals, WN_2 may be structurally isotypic with 3R−MoN_2 and, hence, a promising catalyst candidate, although an *R*3 structure has previously been reported.[33] The crystal structure of WN_2, however, has not been well resolved because the sample used in ref 33, prepared by evaporating W filaments in atmospheres of N_2, is poorly crystalline. More studies are required to resolve the structure of WN_2. The ternary nitrides of $LiMoN_2$ and $LiWN_2$ can be another group of materials with good catalytic activities. They also crystallize in a *R*3m structure, which can simply be viewed as the intercalation of Li ions into the interlayer of XN_2 to form octahedrally coordinated $[LiN_6]$.[42,60] These ternary nitrides are thermodynamically more favorable than binary 3R−MoN_2. For example, at atmospheric pressure, the degassing temperature of $LiMoN_2$ (~1023 K)[41] is ~20% higher than that of 3R−MoN_2 (~850 K). This high thermal stability may make them robust catalyst in high-temperature catalytic application.

CONCLUSIONS

In summary, we have successfully synthesized a novel molybdenum nitride compound, 3R−MoN_2, which has the rhombohedral MoS_2 structure, through a high *P*−*T* route of solid-state ion-exchange. 3R−MoN_2 adopts a peculiar $4d^{2.5}$ electron configuration with a non-integral valence of +3.5 for Mo ions. Most importantly, 3R−MoN_2 exhibits superior catalytic activities and high hydrogenation selectivity over MoS_2 in the hydrodesulfurization of dibenzothiophene. Further, the hydrogenation selectivity of this nitride can be greatly improved when the *h*BN impurity is present. 3R−MoN_2 is also catalytically more active and efficient than δ−MoN in the sour methanation of syngas. Hence, this compound holds great promise as the next-generation catalyst for a wide range of applications. The new nitride can be synthesized at a moderately high pressure of 3.5 GPa, making it feasible for massive and industrial-scale production.

ASSOCIATED CONTENT

Supporting Information

Detailed sample characterizations (including XRD, SEM, EDX, NPD, and XPS measurements) and measurements on phase stability, density, and catalytic properties. This material is available free of charge via the Internet at http://pubs.acs.org.

AUTHOR INFORMATION

Corresponding Authors

*ShanminWang@gmail.com
*gehui@sxicc.ac.cn
*Yusheng.Zhao@UNLV.edu

Notes

The authors declare no competing financial interest.

ACKNOWLEDGMENTS

This work was partially supported by UNLV High Pressure Science and Engineering Center (HiPSEC), which is a DOE NNSA Center of Excellence operated under Cooperative Agreement DE-FC52-06NA27684, and UNLV start-up funding to Y.Z. The work was also partially supported by the NSF of China (No. 21473231). Initial work was supported by Los Alamos National Laboratory, which is operated by Los Alamos National Security LLC under DOE Contract DE-AC52-6NA25396. Use of the ORNL's Spallation Neutron Source at B1 beamline (NOMAD) was sponsored by the Scientific User Facilities Division, DOE−BES. The work was also partially supported by the Strategic Priority Research Program of the CAS for clean and efficient utilization of low−rank Coal, under Grant No. XDA07020400.

REFERENCES

(1) Song, C. *Catal. Today* **2003**, *86*, 211.
(2) Anand, M.; Sughrue, E. L.; Yao, J. MoS2 Catalyst for the Conversion of Sugar Alcohol to Hydrocarbons. WO Patent WO/2012/112190, 2012.
(3) Voiry, D.; Yamaguchi, H.; Li, J.; Silva, R.; Alves, D. C. B.; Fujita, T.; Chen, M.; Asefa, T.; Shenoy, V. B.; Eda, G.; Chhowalla, M. *Nat. Mater.* **2013**, *12*, 850.
(4) Bernardi, M.; Palummo, M.; Grossman, J. C. *Nano Lett.* **2013**, *13*, 3664.
(5) Wang, S.; Zhang, J.; He, D.; Zhang, Y.; Wang, L.; Xu, H.; Wen, X.; Ge, H.; Zhao, Y. *J. Phys. Chem. Solids* **2014**, *75*, 100.
(6) Jaramillo, T. F.; Jørgensen, K. P.; Bonde, J.; Nielsen, J. H.; Horch, S.; Chorkendorff, I. *Science* **2007**, *317*, 100.
(7) Tye, C. T.; Smith, K. J. *Top. Catal.* **2006**, *37*, 129.
(8) Huang, Z. D.; Bensch, W.; Kienle, L.; Fuentes, S.; Alonso, G.; Ornelas, C. *Catal. Lett.* **2008**, *122*, 57.
(9) Song, C.; Ma, X. In *Practical Advances in Petroleum Processing*; Hsu, C., Robinson, P., Eds.; Springer: New York, 2006; p 317.
(10) Abe, H.; Cheung, T. K.; Bell, A. T. *Catal. Lett.* **1993**, *21*, 11.
(11) Tabata, M.; Maeda, K.; Higashi, M.; Lu, D.; Takata, T.; Abe, R.; Domen, K. *Langmuir* **2010**, *26*, 9161.
(12) Chen, W.-F.; Muckerman, J. T.; Fujita, E. *Chem. Commun.* **2013**, *49*, 8896.
(13) Zhao, Y.; Kamiya, K.; Hashimoto, K.; Nakanishi, S. *J. Am. Chem. Soc.* **2015**, *137*, 110.
(14) Neylon, M. K.; Choi, S.; Kwon, H.; Curry, K. E.; Thompson, L. T. *Appl. Catal., A* **1999**, *183*, 253.
(15) Cao, B.; Veith, G. M.; Neuefeind, J. C.; Adzic, R. R.; Khalifah, P. G. *J. Am. Chem. Soc.* **2013**, *135*, 19186.

DOI: 10.1021/jacs.5b01446
J. Am. Chem. Soc. 2015, 137, 4815−4822

(16) Pierson, H. O. In *Handbook of Refractory Carbides & Nitrides: Properties, Characteristics, Processing and Applications*; William Andrew: Burlington, 1996.
(17) Machon, D.; Daisenberger, D.; Soignard, E.; Shen, G.; Kawashima, T.; Takayama-Muromachi, E.; McMillan, P. F. *Phys. Status Solidi A* **2006**, *203*, 831.
(18) Troitskaya, N. V.; Pinsker, Z. G. *Sov. Phys. Crystallogr.* **1959**, *4*, 33.
(19) Ganin, A. Y.; Kienle, L.; Vajenine, G. V. *J. Solid State Chem.* **2006**, *179*, 2339.
(20) Salamat, A.; Hector, A. L.; Kroll, P.; McMillan, P. F. *Coord. Chem. Rev.* **2013**, *257*, 2063.
(21) Zerr, A.; Miehe, G.; Riedel, R. *Nat. Mater.* **2003**, *2*, 185.
(22) Salamat, A.; Hector, A. L.; Gray, B. M.; Kimber, S. A. J.; Bouvier, P.; McMillan, P. F. *J. Am. Chem. Soc.* **2013**, *135*, 9503.
(23) Zerr, A.; Miehe, G.; Li, J.; Dzivenko, D. A.; Bulatov, V. K.; Hoefer, H.; Bolfan-Casanova, N.; Fialin, M.; Brey, G.; Watanabe, T.; Yoshimura, M. *Adv. Funct. Mater.* **2009**, *19*, 2282.
(24) Salamat, A.; Woodhead, K.; Shah, S. I. U.; Hector, A. L.; McMillan, P. F. *Chem. Commun.* **2014**, *50*, 10041.
(25) Crowhurst, J. C.; Goncharov, A. F.; Sadigh, B.; Evans, C. L.; Morrall, P. G.; Ferreira, J. L.; Nelson, A. J. *Science* **2006**, *311*, 1275.
(26) Young, A. F.; Sanloup, C.; Gregoryanz, E.; Scandolo, S.; Hemley, R. J.; Mao, H.-k. *Phys. Rev. Lett.* **2006**, *96*, 155501.
(27) Kawamura, F.; Yusa, H.; Taniguchi, T. *Appl. Phys. Lett.* **2012**, *100*, 251910.
(28) Wang, S.; Yu, X.; Zhang, J.; Chen, M.; Zhu, J.; Wang, L.; He, D.; Lin, Z.; Zhang, R.; Leinenweber, K.; Zhao, Y. *Phys. Rev. B* **2012**, *86*, 064111.
(29) Chen, M.; Wang, S.; Zhang, J.; He, D.; Zhao, Y. *Chem.—Eur. J.* **2012**, *18*, 15459.
(30) Wang, S.; He, D.; Wang, W.; Lei, L. *High Pressure Res.* **2009**, *29*, 806.
(31) Neuefeind, J.; Feygenson, M.; Carruth, J.; Hoffmann, R.; Chipley, K. K. *Nucl. Instrum. Methods Phys. Res., Sect. A* **2012**, *287*, 68.
(32) Toby, B. H. *J. Appl. Crystallogr.* **2001**, *34*, 210.
(33) Langmuir, I. *J. Am. Chem. Soc.* **1913**, *35*, 931.
(34) Brunauer, S.; Emmett, P. H.; Teller, E. *J. Am. Chem. Soc.* **1938**, *60*, 309.
(35) Burch, R.; Collins, A. *Applied Catalysis* **1985**, *17*, 273.
(36) Alvarez, L.; Espino, J.; Ornelas, C.; Rico, J. L.; Cortez, M. T.; Berhault, G.; Alonso, G. *J. Mol. Catal. A: Chem.* **2004**, *210*, 105.
(37) Jiang, M.; Wang, B.; Yao, Y.; Li, Z.; Ma, X.; Qin, S.; Sun, Q. *Catal. Sci. Technol.* **2013**, *3*, 2793.
(38) Wang, S.; Yu, X.; Lin, Z.; Zhang, R.; He, D.; Qin, J.; Zhu, J.; Han, J.; Wang, L.; Mao, H.-K.; Zhang, J.; Zhao, Y. *Chem. Mater.* **2012**, *24*, 3023.
(39) Karam, R.; Ward, R. *Inorg. Chem.* **1970**, *9*, 1385.
(40) Wriedt, H. A. *Bull. Alloy Phase Diagrams* **1989**, *10*, 358.
(41) Elder, S. H.; Doerrer, L. H.; Disalvo, F. J.; Parise, J. B.; Guyomard, D.; Tarascon, J. M. *Chem. Mater.* **1992**, *4*, 928.
(42) Herle, P. S.; Hegde, M. S.; Vasanthacharya, N. Y.; Gopalakrishnan, J.; Subbanna, G. N. *J. Solid State Chem.* **1994**, *112*, 208.
(43) Hahn, T. *International Tables for Crystallography, Brief Teaching ed. of Vol. A: Space Group Symmetry*; Springer, 2002.
(44) Sears, V. F. *Neutron News* **1992**, *3*, 26.
(45) Liang, K. S.; Chianelli, R. R.; Chien, F. Z.; Moss, S. C. *J. Non-Cryst. Solids* **1986**, *79*, 251.
(46) Peng, Y.; Meng, Z.; Zhong, C.; Lu, J.; Yu, W.; Yang, Z.; Qian, Y. *J. Solid State Chem.* **2001**, *159*, 170.
(47) Chianelli, R. R.; Prestridge, E. B.; Pecoraro, T. A.; Deneufville, J. P. *Science* **1979**, *203*, 1105.
(48) Wang, S.; Wang, Z.; Qin, J.; Wang, W.; Li, W.; He, D. *Mater. Chem. Phys.* **2011**, *130*, 170.
(49) Warren, B. E. *Phys. Rev.* **1941**, *59*, 693.
(50) Bowden, F. L.; Heveldt, P. F.; Watson, D. J. In *Inorganic Chemistry of the Transition Elements*, Vol. *6*; Johnson, B. F. G., Ed.; The Royal Society of Chemistry: London, 1978; Vol. *6*, p 1.
(51) Bull, C. L.; McMillan, P. F.; Soignard, E.; Leinenweber, K. *J. Solid State Chem.* **2004**, *177*, 1488.
(52) Maugé, F.; Lamotte, J.; Nesterenko, N. S.; Manoilova, O.; Tsyganenko, A. A. *Catal. Today* **2001**, *70*, 271.
(53) Song, C.; Nihonmatsu, T.; Nomura, M. *Ind. Eng. Chem. Res.* **1991**, *30*, 1726.
(54) Shimura, M.; Shiroto, Y.; Takeuchi, C. *Ind. Eng. Chem. Fundam.* **1986**, *25*, 330.
(55) Valencia, D.; Klimova, T. *Appl. Catal. B: Environ.* **2013**, *129*, 137.
(56) Huang, Z. D.; Bensch, W.; Kienle, L.; Fuentes, S.; Alonso, G.; Ornelas, C. *Catal. Lett.* **2009**, *127*, 132.
(57) Zeng, T.; Wen, X.-D.; Li, Y.-W.; Jiao, H. *J. Phys. Chem. B* **2005**, *109*, 13704.
(58) Cho, A.; Lee, J. J.; Koh, J. H.; Wang, A.; Moon, S. H. *Green Chem.* **2007**, *9*, 620.
(59) Young, A. F.; Sanloup, C.; Gregoryanz, E.; Scandolo, S.; Hemley, R. J.; Mao, H. K. *Phys. Rev. Lett.* **2006**, *96*, 155501.
(60) Maoujoud, M.; Jardinier-Offergeld, M.; Bouillon, F. *Appl. Surf. Sci.* **1993**, *64*, 81.

DOI: 10.1021/jacs.5b01446
J. Am. Chem. Soc. 2015, 137, 4815−4822